



Title	A 60 year record of atmospheric aerosol depositions preserved in a high-accumulation dome ice core, southeast Greenland
Author(s)	Iizuka, Yoshinori; Uemura, Ryu; Fujita, Koji; Hattori, Shohei; Seki, Osamu; Miyamoto, Chihiro; Suzuki, Toshitaka; Yoshida, Naohiro; Motoyama, Hideaki; Matoba, Sumito
Citation	Journal of Geophysical Research: Atmospheres, 123(1), 574-589 https://doi.org/10.1002/2017JD026733
Issue Date	2018-01-04
Doc URL	http://hdl.handle.net/2115/70919
Rights	Copyright 2018 American Geophysical Union.
Type	article
File Information	Iizuka_et_al-2018-Journal_of_Geophysical_Research__Atmospheres.pdf



[Instructions for use](#)

Journal of Geophysical Research: Atmospheres**RESEARCH ARTICLE**

10.1002/2017JD026733

This article is a companion to Furukawa et al. (2017) <https://doi.org/10.1002/2017JD026716>.

Key Points:

- A Greenland ice core from a high-accumulation area records the seasonal ion fluxes over the past 60 years without postdepositional effect
- Sea salt and dust fluxes increased after 2000, indicating increased contribution of local regions in Greenland and around the ocean
- Sulfate flux responds to the decreasing trend of SO_x emissions, but the nitrate flux does not follow the decrease in NO_x

Correspondence to:

Y. Iizuka and S. Matoba,
iizuka@lowtem.hokudai.ac.jp;
matoba@lowtem.hokudai.ac.jp

Citation:

Iizuka, Y., Uemura, R., Fujita, K., Hattori, S., Seki, O., Miyamoto, C., ... Matoba, S. (2018). A 60 year record of atmospheric aerosol depositions preserved in a high-accumulation dome ice core, Southeast Greenland. *Journal of Geophysical Research: Atmospheres*, 123, 574–589. <https://doi.org/10.1002/2017JD026733>

Received 28 FEB 2017

Accepted 6 DEC 2017

Accepted article online 13 DEC 2017

Published online 4 JAN 2018

A 60 Year Record of Atmospheric Aerosol Depositions Preserved in a High-Accumulation Dome Ice Core, Southeast Greenland

Yoshinori Iizuka¹ , Ryu Uemura² , Koji Fujita³ , Shohei Hattori⁴ , Osamu Seki¹, Chihiro Miyamoto⁵, Toshitaka Suzuki⁶, Naohiro Yoshida^{4,7} , Hideaki Motoyama⁸ , and Sumito Matoba¹

¹Institute of Low Temperature Science, Hokkaido University, Sapporo, Japan, ²Department of Chemistry, Biology, and Marine Science, Faculty of Science, University of the Ryukyus, Nishihara, Japan, ³Graduate School of Environmental Studies, Nagoya University, Nagoya, Japan, ⁴Department of Chemical Science and Engineering, School of Materials and Chemical Technology, Tokyo Institute of Technology, Yokohama, Japan, ⁵Department of Earth and Planetary Science, Graduate School of Science, The University of Tokyo, Tokyo, Japan, ⁶Department of Earth and Environmental Sciences, Faculty of Science, Yamagata University, Yamagata, Japan, ⁷Earth-Life Science Institute, Tokyo Institute of Technology, Yokohama, Japan, ⁸National Institute of Polar Research, Tokyo, Japan

Abstract The Southeastern Greenland Dome (SE-Dome) has both a high elevation and a high accumulation rate ($1.01 \text{ m we yr}^{-1}$), which are suitable properties for reconstructing past environmental changes with a high time resolution. For this study, we measured the major ion fluxes in a 90 m ice core drilled from the SE-Dome region in 2015 and present the records of annual ion fluxes from 1957 to 2014. From 1970 to 2010, the trend of nonsea-salt (nss) SO_4^{2-} flux decreases, whereas that for NH_4^+ increases, tracking well with the anthropogenic SO_x and NH_3 emissions mainly from North America. The result suggests that these fluxes reflect histories of the anthropogenic SO_x and NH_3 emissions. In contrast, the decadal trend of NO_3^- flux differs from the decreasing trend of anthropogenic NO_x emissions. Although the cause of this discrepancy remains unclear, it may be related to changes in particle formation processes and chemical scavenging rates caused by an increase in sea salt and dust and/or a decrease in nss SO_4^{2-} . We also find a high average NO_3^- flux ($1.13 \text{ mmol m}^{-2} \text{ yr}^{-1}$) in the ice core, which suggests a negligible effect from postdepositional NO_3^- loss. Thus, the SE-Dome region is an excellent location for reconstructing nitrate fluxes. Over a decadal time scale, our NO_3^- flux record is similar to those from other ice cores in Greenland high-elevation sites, suggesting that NO_3^- concentration records from these ice cores are reliable.

1. Introduction

The years after 1950 include a high-pollution period involving significant emissions of anthropogenic aerosols and greenhouse gases, and then from the 1970s a subsequent conservation period of global environment regulations (e.g., IPCC, 2013). Examples of such anthropogenic aerosols that were regulated include precursors of SO_x and NO_x (NO_y) (Crippa et al., 2016). SO_x and NO_x are converted to strong acids (H_2SO_4 and HNO_3) in the atmosphere and cause environmental destruction as acid rain (Likens et al., 1996; Stoddard et al., 1999). Sulfate and nitrate in the atmosphere also become microparticles in the atmosphere (secondary aerosols) and decrease the surface air temperature by both direct and indirect effects of radiative forcing (Andreae & Rosenfeld, 2008; Pöschl, 2005).

Recent changes in SO_x and NO_x emissions are mainly attributed to anthropogenic activity (Emission Database for Global Atmospheric Research (EDGAR) project; see e.g., Crippa et al., 2016). As a result, time series of the emissions differ by country both quantitatively and trend-wise. Emissions from Asia are still growing very fast, with both China and India surpassing that from the United States and Western Europe for SO_x . The rate of increase in emissions from China dramatically slows after 2006, but not so for India. Thus, it is important to better understand historical changes in both source and emission of SO_x and NO_x to evaluate the impact of anthropogenic activity on Earth's climate and environment.

Past SO_x and NO_x (NO_y) history can be reconstructed from ice cores drilled from ice sheets and glaciers (Legrand & Mayewski, 1997; Petit et al., 1999; Plummer et al., 2012; Röthlisberger et al., 2002; Wolff et al., 2006). These compounds are preserved as SO_4^{2-} and NO_3^- in ice sheets and glaciers after wet or dry

deposition to surface snow in the polar and high-mountain regions (Legrand et al., 1988; Legrand & Mayewski, 1997). In the Arctic, wet deposition produces about 90% of the black carbon, sulfate, and dust depositions (Breider et al., 2014), which suggests that wet deposition probably also produces the nitrate deposition due to nitrate being a more hygroscopic material (e.g., IPCC, 2013).

An advantage of using ice cores to reconstruct SO_x and NO_x history is the long-term nature of their record. Previous ice core studies (e.g., Fischer et al., 1998; Patris et al., 2002) have reported changes in the concentration of SO_4^{2-} from Greenland ice cores over the past 300 years. The SO_4^{2-} records in Greenland ice cores agree with historical changes in anthropogenic SO_x emissions from North America, indicating that Greenland ice cores are a useful archive to evaluate past emissions of anthropogenic SO_4^{2-} from North America. However, for the period after 1970–1980, when SO_x emissions were a maximum, few studies (e.g., Maselli et al., 2017; Plummer et al., 2012) have reconstructed the SO_4^{2-} records.

In contrast to SO_4^{2-} , preservation of NO_3^- in snow is reduced by photolysis, volatilization during snow sublimation, and stress desorption due to snow grain growth particularly at low accumulation rates (Dibb & Jaffrezo, 1997; Geng et al., 2015; Röhlisberger et al., 2002; Wagnon et al., 1999; Zatko et al., 2016). For instance, ice from the top few centimeters in inland Antarctica loses about 90% of its NO_3^- (Iizuka et al., 2004; Wagnon et al., 1999). Inland Greenland may have a comparable loss to photolysis (Zatko et al., 2016), making it difficult to determine past trends in NO_x from ice cores. So reconstructing historical variations of NO_x concentrations in the atmosphere from ice core records is still highly uncertain.

In areas where the top few centimeters are quickly buried by new snowfall, the NO_3^- recorded is better preserved. Hence, it is vital to use ice core data from a high-accumulation area to obtain a reliable record of NO_3^- flux. This vital feature tends to compete against a more general requirement for precise reconstruction, specifically the use of ice from a region with minimal ice advection, such as a dome region. Due to this latter requirement, many ice cores have been drilled in ice sheet domes such as Dome Fuji (Watanabe et al., 2003), EPICA DML (EPICA community members, 2006), EPICA Dome C (EPICA community members, 2004), GRIP (Greenland Ice-core Project Members, 1993), GISP2 (Grootes et al., 1993), and NGRIP (North Greenland Ice Core Project Members, 2004). However, most domes are in a highland polar region, which tend to be dry and thus have a low accumulation rate—a disadvantage for NO_3^- reconstruction.

A 90.45 m depth ice core was obtained at a high-elevation (above 3,000 m above sea level (asl)) dome site in southeast Greenland called SE-Dome (Iizuka et al., 2016). The SE-Dome region has the distinct characteristic of having the highest accumulation rate of any known dome of the Antarctic and Greenland ice sheets, a value in water equivalent (we) of $1.01 \pm 0.22 \text{ m yr}^{-1}$ (1960–2014), which is about 4 times that of a typical inland Greenland ice core and about 30 times that of a typical inland Antarctic ice core (Iizuka et al., 2017). Moreover, the precise age scale for the SE-Dome ice core allows us to investigate seasonal variations of the climatic records from 1960 to 2014 (Furukawa et al., 2017). In this paper, we argue that the SE-Dome ice core preserves the NO_3^- flux better than previous polar ice records, and we evaluate the SO_4^{2-} and NO_3^- record against known emissions of SO_x and NO_x over the past 60 years.

2. Sample and Analytical Methods

2.1. SE-Dome Ice Core and Age Scale

We used a 90.45 m depth ice core obtained at a dome site on the SE-Dome (67.18°N , 36.37°W , 3,170 m asl). The annual mean temperature at the SE-Dome is -20.9°C , based on 20 m deep firn-temperature measurements (Iizuka et al., 2017). For a time scale, we use the SEIS2016 age scale for 1960–2014, which is determined by the oxygen-isotope matching method (Furukawa et al., 2017). The SEIS2016 scale has been carefully evaluated with independent age markers, and its precision is within a few months. From 1957 to 1959, we regard Na^+ maxima as marking depths of February precipitation. Then, linear interpolation is adapted to convert the depths to the beginning of the year. The measured number of samples is 1637 from 1957 to 2014, corresponding to 29 samples per year on average.

2.2. Ion Concentration Measurements

In a cold room (Institute of Low Temperature Science, Hokkaido University, Japan), we divided the ice core into 50 mm depth sections. Above 12.5 m, the low firn density gave a low sampling volume, so we instead

divided this shallow part of core into 100 mm sections. The samples were divided using a clean ceramic knife in a cold clean room (class 10,000), put into a cleaned polyethylene bottle, and then melted in the bottle at room temperature in a clean room. The ion concentrations of CH_3SO_3^- , Cl^- , SO_4^{2-} , NO_3^- , Na^+ , Ca^{2+} , NH_4^+ , Mg^{2+} , and K^+ were measured by ion chromatography (Thermo Scientific ICS-2100; column is Dionex CS-12A, and eluent is 20 mM MSA for cation; column is Dionex AS-14A, and eluent is 23 mM NaOH for anion). The injection volumes are 1,000 μL for anion and 500 μL for cation. Most CH_3SO_3^- and K^+ concentrations were below the detection limit and thus not discussed in this paper. Analytical precision of the ion concentration is 10%. To confirm that any large peak in ion concentration is not caused by analytical errors, significantly different values from two adjacent samples (based on a 3-point running standard deviation ($>3\sigma$)) were checked by remeasuring the ice sample from the same depth. To detect NH_4^+ accurately, the surface decontamination and sample melting were done within 1 week and 1 day, respectively, of the ion-chromatography measurement. For SO_4^{2-} and Ca^{2+} , their nonsea-salt (nss) fractions were calculated as follows. If all Na^+ is assumed to come from sea salt (ss), then the sea-salt fraction is $[\text{nssSO}_4^{2-}] = 0.060 [\text{Na}^+]$ and $[\text{nssCa}^{2+}] = 0.022 [\text{Na}^+]$. Thus, $[\text{nssSO}_4^{2-}] = [\text{SO}_4^{2-}] - [\text{ssSO}_4^{2-}]$; $[\text{nssCa}^{2+}] = [\text{Ca}^{2+}] - [\text{ssCa}^{2+}]$.

2.3. Flux Estimation

The seasonal ion fluxes are based on the seasonal average value of each ion concentration multiplied by the seasonal accumulation rate. The seasonal boundaries are 1 March, 1 June, 1 September, and 1 December for spring (MAM), summer (JJA), autumn (SON), and winter (DJF). The annual ion fluxes are based on the sum of four seasons with the boundary of 1 March. These annual and seasonal accumulation rates are precisely estimated based on the SEIS2016 age scale (Furukawa et al., 2017). This method is similar to that used previously for the NO_3^- concentration of the SIGMA-D ice core in northwestern Greenland. In that study, the annual NO_3^- flux from 1950 to 2013 is obtained using the annual accumulation rate (from Matoba et al., 2015) multiplied by the annual average value of NO_3^- concentration.

2.4. Isotope Measurement

The nitrogen isotopic composition of NO_3^- is $\delta^{15}\text{N}$, where $\delta X = R_{\text{Sample}}/R_{\text{Standard}} - 1$ and R is $^{15}\text{N}/^{14}\text{N}$ in the sample or in the standard (atmospheric N_2 for the nitrogen isotope). Nitrogen isotopic composition of nitrate in surface snow at the SE-Dome region was measured according to method described in Hattori et al. (2016). NO_3^- in the surface snow samples collected in Iizuka et al. (2016) were concentrated and separated from other ions using the ion-chromatographic method described in Ishino et al. (2017). NO_3^- was converted to N_2O using a strain of denitrifying bacteria that has no N_2O reductase. The produced N_2O was then separated from other species by chemical traps and gas chromatography and decomposed to O_2 and N_2 with a microwave-induced plasma. The isotopic ratios of each gas were measured by a MAT253 isotope-ratio mass spectrometer (Thermo Fisher Scientific, Bremen, Germany). The analytical uncertainty of the measurements here is 0.3‰ for $\delta^{15}\text{N}$ values.

2.5. Backward Trajectory Analysis

To investigate source regions of the chemical species preserved in the ice core, transport pathways of air masses are analyzed using the HYSPLIT model (Hybrid Single-Particle Lagrangian Integrated Trajectory), which is distributed by NOAA (National Oceanographic and Atmospheric Administration) (Stein et al., 2015). Points at 0, 500, 1,000, and 1,500 m above ground level (agl), which correspond to 1,550, 2,050, 2,550 and 3,050 m asl in the model, are set as starting points of the 30 day backward trajectories. The probability distribution of the air mass at altitudes between 0 and 1,500 m agl is calculated at a 1° resolution. We assume wet deposition for the preserved aerosols. And thus, the probability is weighted by the daily amount of precipitation when the air mass arrived at the core site. We used the daily precipitation in the reanalysis data sets of ERA-40 and ERA-Interim, both produced by European Centre for Medium-Range Weather Forecasts (Dee et al., 2011; Uppala et al., 2005). To maintain consistency among the two precipitation products for the whole period (1958–2014), the daily precipitation of ERA-40 (p40) is calibrated with that of ERA-Interim (pi) by a linear regression obtained for the period 1979–2001 ($\text{pi} = 1.36 \text{ p40}$, $R^2 = 0.862$, $p < 0.001$). From the probability distribution, we also calculate the regional contribution for each day and for all land regions in the Northern Hemisphere, which is divided into 13 regions in the national boundary data (<http://www.naturalearthdata.com/>, last access: 5 June 2017).

Table 1
Ion Concentrations Over the Entire Core ($\mu\text{mol L}^{-1}$)

	Cl^-	SO_4^{2-}	NO_3^-	Na^+	NH_4^+	Mg^{2+}	Ca^{2+}
Average value (standard deviation)	0.59 (0.42–0.85)	0.67 (0.48–0.94)	0.94 (0.70–1.26)	0.47 (0.31–0.72)	0.70 (0.46–1.08)	0.16 (0.10–0.26)	0.29 (0.19–0.45)

Note. The statistical values are calculated assuming a lognormal distribution.

3. Results and Discussion

3.1. General Characteristics of Ion Concentrations in SE-Dome Ice Core

The major cation is NH_4^+ , with a core average of $0.70 \mu\text{mol L}^{-1}$, and the major anion is NO_3^- , at $0.94 \mu\text{mol L}^{-1}$ (Table 1). These values correspond well to those in surface snow (Iizuka et al., 2016). Moreover, in their time series (Figure 1), these two ions correlate strongly with $r^2 = 0.62$ (Table 2). The table also shows that NH_4^+ correlates with SO_4^{2-} ions ($r^2 = 0.75$), whereas Cl^- , Na^+ , and Mg^{2+} ions strongly correlate with each other ($r^2 > 0.70$). Summing values in Table 1, the total anion concentration ($2.87 \mu\text{eq L}^{-1}$) is higher than that of the total cation concentration ($2.07 \mu\text{eq L}^{-1}$), indicating that acid compounds (HCl , H_2SO_4 , and HNO_3) are also contained in this ice.

These ion species can be separated into three groups using principal component analysis. Table 3 shows their principal component loadings. In the first component, Cl^- (-0.92), Na^+ (-0.87), and Mg^{2+} (-0.95) have high absolute loading values. Other than their strong correlations, they have ratios nearly equal to the sea-salt ratios (Table 1), suggesting that Cl^- , Na^+ , and Mg^{2+} mainly originate from sea salt. Previous studies suggest

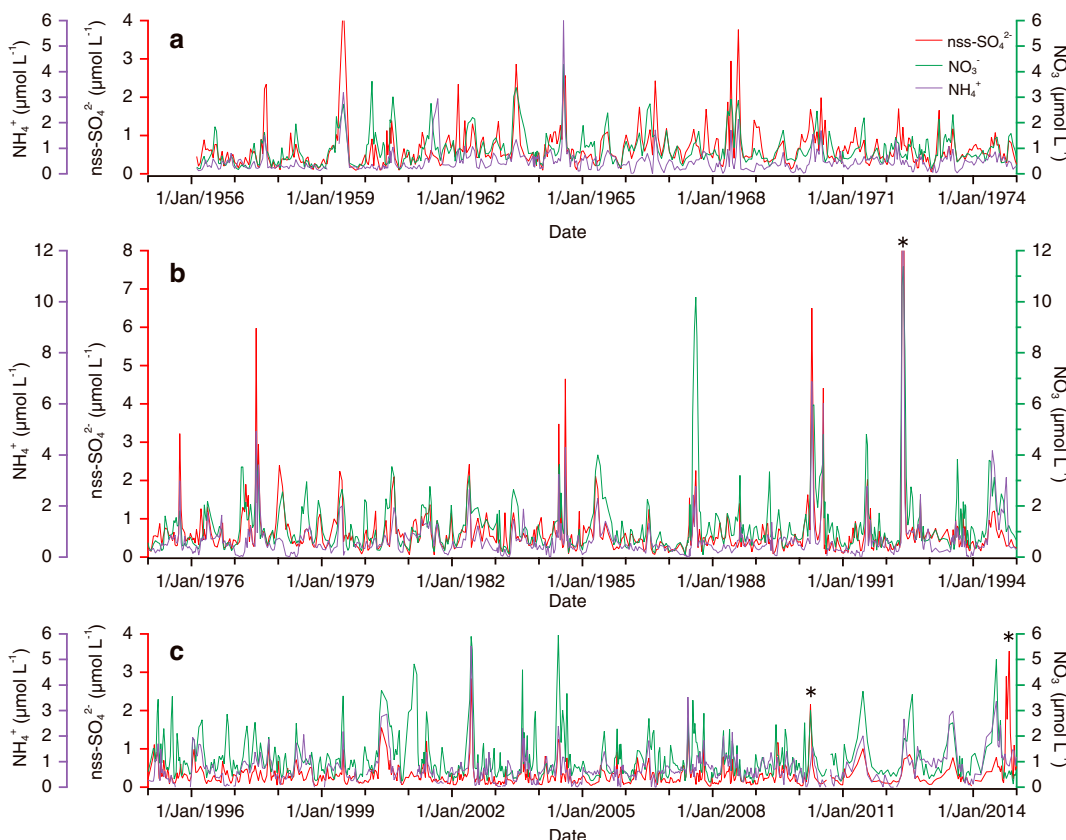


Figure 1. Time series of NO_3^- (green), nssSO_4^{2-} (red), and NH_4^+ (purple) concentrations ($\mu\text{mol L}^{-1}$). (a) 1957–1975, (b) 1975–1995, and (c) 1995–2015. The asterisks in 1992, 2010, and 2014 are volcanic contribution of Pinatubo (Philippines), Eyjafjallajökull (Iceland), and Bardarbunga (Iceland), respectively (Iizuka et al., 2017). The Pinatubo signature has peak NO_3^- , nssSO_4^{2-} , and NH_4^+ values of 11.38 , 13.74 , and $17.35 \mu\text{mol L}^{-1}$, respectively.

Table 2

Correlation Coefficients Between Ion Species

	Cl^-	SO_4^{2-}	NO_3^-	Na^+	NH_4^+	Mg^{2+}	Ca^{2+}
Cl^-	—	0.14	0.06	0.97	0.07	0.72	0.33
SO_4^{2-}	0.25	—	0.59	0.08	0.75	0.19	0.19
NO_3^-	0.38	0.51	—	-0.05	0.62	0.06	0.12
Na^+	0.95	0.23	0.23	—	0.01	0.70	0.38
NH_4^+	0.53	0.46	0.62	0.49	—	0.13	0.19
Mg^{2+}	0.78	0.18	0.36	0.72	0.31	—	0.64
Ca^{2+}	0.61	0.01	0.21	0.60	0.33	0.71	—

Note. Values above the diagonal are between ion concentrations ($n = 1637$), and values below the diagonal are between annual ion fluxes ($n = 57$).

that they have seasonal peaks during winter (e.g., Legrand & Mayewski, 1997; Whitlow et al., 1992). In the second component, SO_4^{2-} (-0.79), NO_3^- (-0.79), and NH_4^+ (-0.85) all have high absolute loading values. They also strongly correlate with each other and are the primary ion species in the SE-Dome ice core. In the third component, only Ca^{2+} (-0.85) has a high absolute loading value. This component can be explained as a soluble terrestrial contribution (e.g., Legrand & Mayewski, 1997; Whitlow et al., 1992).

The cumulative contribution ratio (Table 3), summed from the first to third components, is 89.0% of the total contribution, indicating that these three components well explain the general characteristics of ion concentrations in the SE-Dome ice core. In the following sections, we discuss the flux fluctuations of the sea-salt and terrestrial components (first and third components), and then the fluctuations of the N and S species in detail (second component).

3.2. Sea Salt and Terrestrial Components

To help determine the sources, we calculated the probability distributions of an air mass arriving at the SE-Dome site. The results in Figure 2, from back trajectory analyses, suggest three main findings. (1) The air mass at upper elevations (1,000 and 1,500 m agl) comes from a broader region than that at lower elevations (0 and 500 m agl). (2) The air mass at lower elevations (0 and 500 m agl) comes not only from the region including southern-southeastern Greenland and the North Atlantic Ocean in the 7 day analysis (Figure 2a) but also from eastern Canada in the 14 and 25 day analyses (Figures 2b and 2c) and from Russia in the 25 day analysis (Figure 2c). (3) The air mass at upper elevations (1,000 and 1,500 m agl) also comes from eastern Canada, as well as from a broad region that includes southern and southeastern Greenland, the North Atlantic Ocean, and northern and western Europe in the 7 and 14 day analyses (Figures 2d and 2e), and also from Russia and northern Alaska in the 25 day analysis (Figure 2f). There is little contribution from East Asia (Japan and China) and India, which are high anthropogenic SO_x , NO_x , and NH_3 emission regions (Crippa et al., 2016).

From the trajectory analyses, we estimate the interannual variability of the regional contributions. Five regions are selected as possible source regions of anthropogenic emission for the SE-Dome site (Figure 3, top). The interannual variability during 1957 to 2014 is smaller than the trajectory counting days (7, 14, and 25 days). The air mass at the lower elevations (0 and 500 m agl) comes from Greenland (7 and 14 days), North America (7 and 14 days), Europe (7, 14, and 25 days), and Russia (7, 14, and 25 days). The air mass at the upper elevations (1,000 and 1,500 m agl) comes mainly from North America and also from Greenland, Europe, and Russia (7, 14, and 25 days).

The Cl^- , Na^+ , and Mg^{2+} fluxes are highly correlated with each other ($r^2 > 0.70$ in Table 2). The ratio of Cl^-/Na^+ (1.25 average) nearly equals the sea-salt ratios (1.18). The back trajectory analyses (Figure 2) suggest that the sea-salt particles are transported from the North Atlantic Ocean. Sporadically high flux peaks occur during (1) winter in

Table 3Statistical Scores From Primary Component Analyses of Cl^- , SO_4^{2-} , NO_3^- , Na^+ , NH_4^+ , Mg^{2+} , and Ca^{2+} Concentrations

	First component	Second component	Third component
Cl^-	-0.92	0.27	0.24
SO_4^{2-}	-0.39	-0.79	0.16
NO_3^-	-0.27	-0.79	0.02
Na^+	-0.87	0.40	0.22
NH_4^+	-0.29	-0.85	0.08
Mg^{2+}	-0.95	0.24	-0.08
Ca^{2+}	-0.51	-0.09	-0.85
Eigenvalue	3.08	2.28	0.87
Cumulative contribution ratio	44.05	76.56	88.99

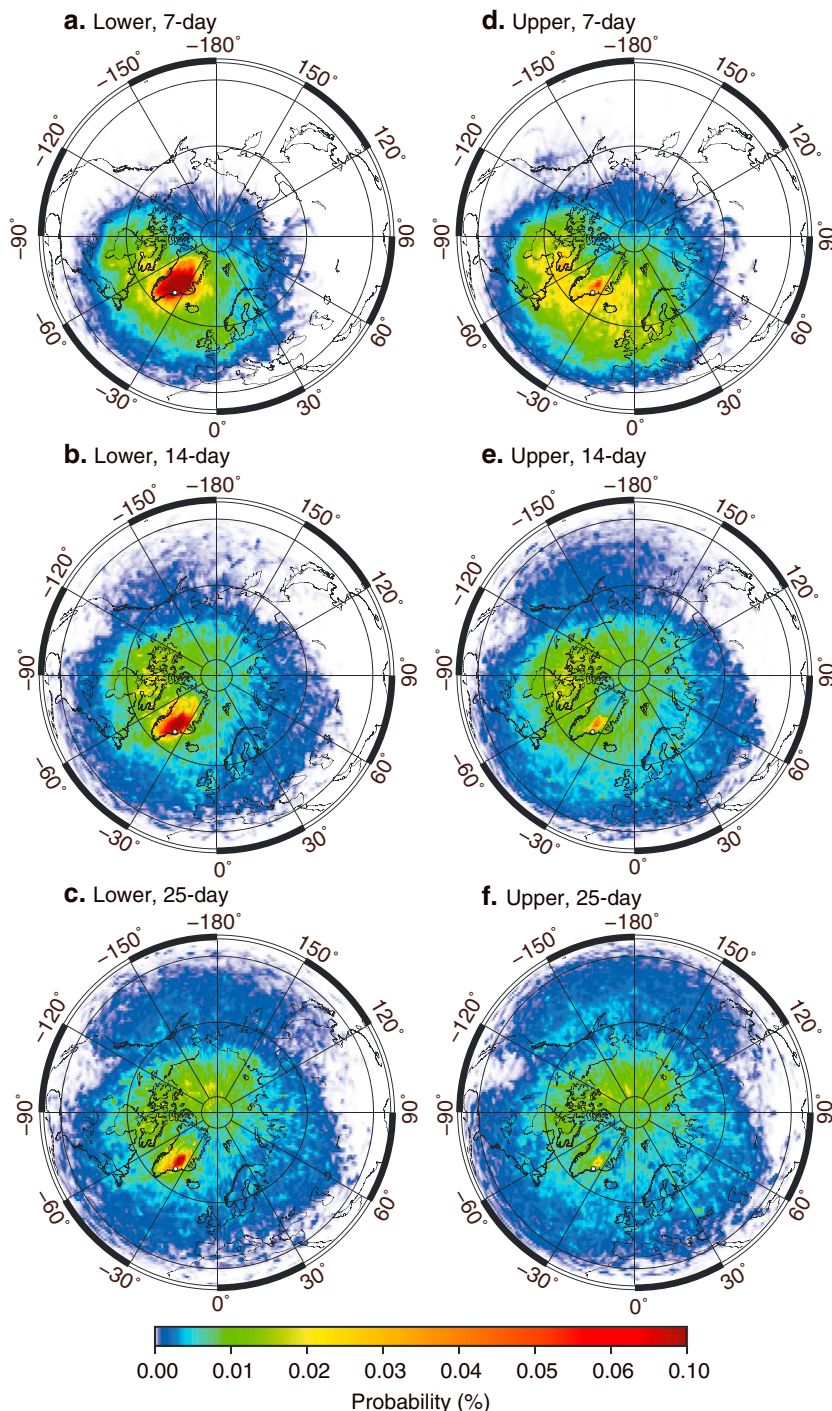


Figure 2. Probability distribution of an air mass arriving at the SE-Dome site from a 25 day 3-D backward-trajectory analysis for two elevations and three terms. The color scale at the bottom. (left column) “Lower” means 0 and 500 m agl, and (right column) “upper” means 1,000 and 1,500 m agl air masses. Trajectory periods are (top row) 7 days, (middle) 14 days, and (bottom) 25 days. Existence of the air mass is weighted by the daily precipitation in reanalysis data sets of ERA-40 and ERA-Interim.

1990–1991, 2003–2004, 2013–2014, and 2014–2015; (2) during spring/summer in 1972, 1979, and 1984; and (3) during autumn in 2007 and 2008 (Figures 4a and 4b). Mainly due to the peaks, the Cl^- and Na^+ fluxes exceed $0.5 \text{ mmol m}^{-2} \text{ yr}^{-1}$ in about half of the years after 2000, indicating an increasing amount of sea salt from the North Atlantic after 2000.

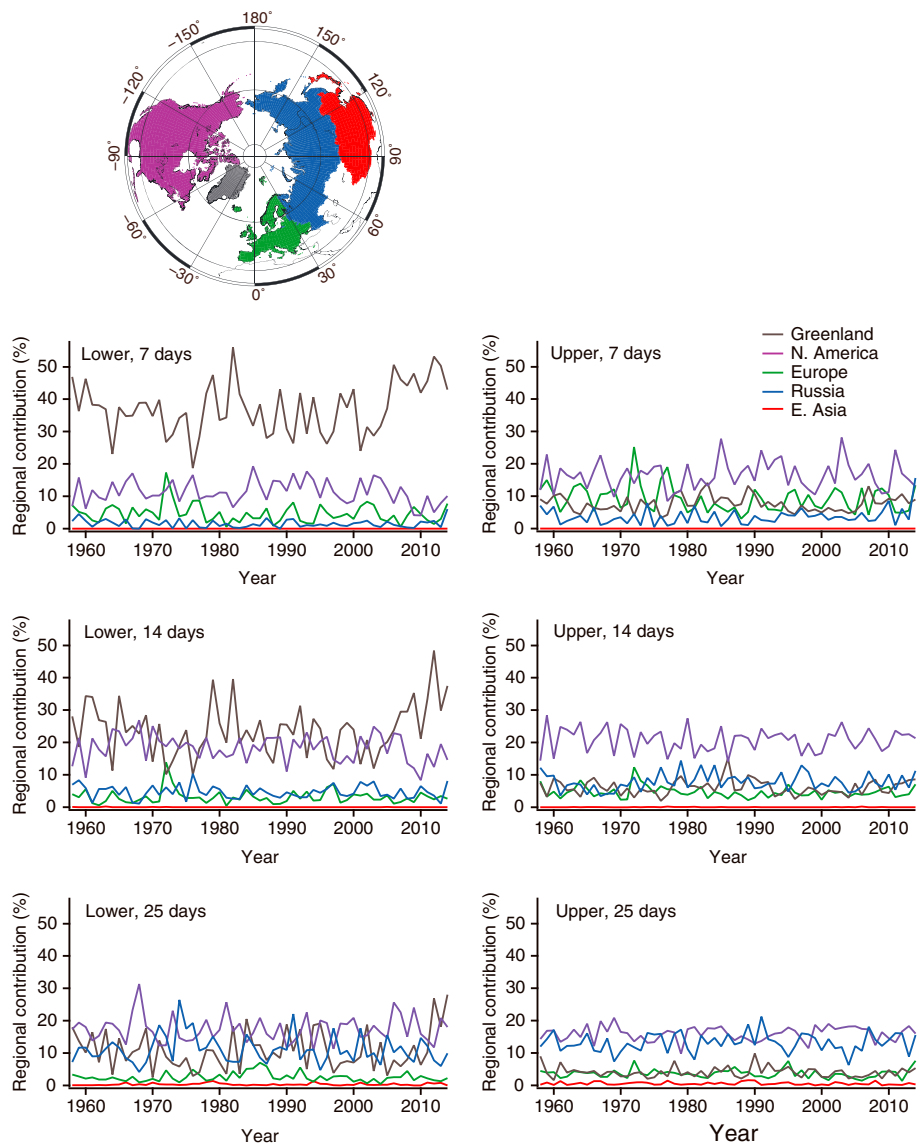


Figure 3. Time series of regional contributions of air mass origins. The regions are shown at the top. Greenland in gray, North America in purple (Canada and the U.S.), Europe in green, Russia in blue (includes Ukraine), and East Asia in red (China and Japan). Each panel corresponds to panels in Figure 2.

The nssCa²⁺ flux is nearly constant from 1957 to 2000 (Figure 4c), but then trends upward till the present. This nssCa²⁺ (and dust) deposited in high-elevation sites of Greenland is thought to originate mainly from Asia, primarily from China deserts (Bory et al., 2003; Fischer et al., 2007; Prospero et al., 2002). However, the flux of Asian dust shows a decreasing trend in recent decades, associated with the warming of Mongolia that represents a northward shift of the westerlies (Nagashima et al., 2016; Zhu et al., 2008), which seems to contradict the increasing trend of nssCa²⁺ flux in SE-Dome. The relatively high nssCa²⁺ fluxes after 2000 may instead link to a local source, such as an increase in land-area exposure around the southeastern Greenland coast. In particular, the retreat rates of ice sheets (marine- and land-terminating) and local glaciers accelerated after 2000 (Bjørk et al., 2012). This retreat acceleration is common in Greenland; for example, van den Broeke et al. (2009) showed a cumulative mass anomaly of the Greenland Ice Sheet and a decreasing trend of ice mass from ~1990 to present. These ice retreats tend to expose more land from snow-covered areas in the coastal regions. Mesoscale wind around the SE-Dome region is mainly from the northeast and/or east regions (Hanna et al., 2006; Moore et al., 2015) where there are many nunataks. Thus, the wind direction and glacial trends suggest a local source of nssCa²⁺.

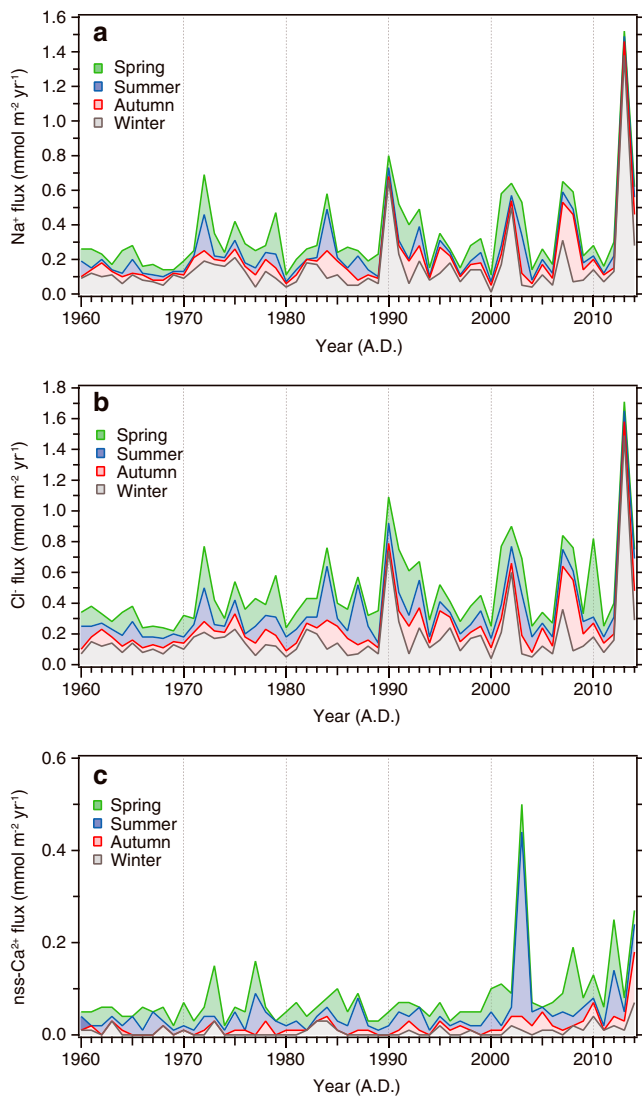


Figure 4. Seasonal ion fluxes ($\text{mmol m}^{-2} \text{yr}^{-1}$). (a) Na^+ , (b) Cl^- , and (c) nssCa^{2+} from 1957 to 2014. Any given year begins with spring, on 1 March. The uncertainty is about 19%.

slightly increasing, with larger peaks during 1987–1995. The highest of these peaks are in 1987 ($2.53 \text{ mmol m}^{-2} \text{yr}^{-1}$), 1990 ($1.92 \text{ mmol m}^{-2} \text{yr}^{-1}$), 1992 ($2.25 \text{ mmol m}^{-2} \text{yr}^{-1}$), and 1995 ($1.78 \text{ mmol m}^{-2} \text{yr}^{-1}$). Outside of this period, the NO_3^- flux remains at $1.0 \pm 0.5 \text{ mmol m}^{-2} \text{yr}^{-1}$ except peaks at 1977 ($1.69 \text{ mmol m}^{-2} \text{yr}^{-1}$) and 2002 ($1.75 \text{ mmol m}^{-2} \text{yr}^{-1}$). The peaks at 1977, 1987, 1990, 1992, 1995, and 2002 arise during spring and/or summer.

Finally, the NH_4^+ flux from 1957 to 2014 shows an increasing trend (Figure 6c). Until the mid-1980s, the NH_4^+ flux sometimes dips below $0.5 \text{ mmol m}^{-2} \text{yr}^{-1}$. But thereafter, it remains between 0.5 and $1.0 \text{ mmol m}^{-2} \text{yr}^{-1}$ except for a few peaks, including 1984 ($1.04 \text{ mmol m}^{-2} \text{yr}^{-1}$), 1990 ($1.19 \text{ mmol m}^{-2} \text{yr}^{-1}$), 1992 ($1.74 \text{ mmol m}^{-2} \text{yr}^{-1}$), 2007 ($1.08 \text{ mmol m}^{-2} \text{yr}^{-1}$), 2008 ($1.03 \text{ mmol m}^{-2} \text{yr}^{-1}$), and 2014 ($1.73 \text{ mmol m}^{-2} \text{yr}^{-1}$). The peaks at 1984 and 1990 occur mainly in summer, but those in 1992, 2007, 2008, and 2014 occur from spring to autumn.

The maximum nssSO_4^{2-} , NO_3^- , and NH_4^+ fluxes are in 1992 and are also notably high around 1990. Prior to about 1995, the NO_3^- flux is at a similar level as the nssSO_4^{2-} flux. Then, after about 1995, the NO_3^- (as well as the NH_4^+) flux exceeds that of nssSO_4^{2-} . The following section examines the NO_3^- record by focusing on the postdepositional loss, the causes of the long-term trend, and comparison with other ice cores.

Micrographs of nonvolatile particles in the SE-Dome ice core support the evidence for a local source. Figure 5 shows that some particles have a diameter exceeding $10 \mu\text{m}$ with a silicon component (indicating silicate minerals). Such huge particles suggest a local dust origin due to their shorter lifetime in the atmosphere. The increases of nssCa^{2+} flux (Figure 4c) occur not only in spring (2001 and 2008) but also in summer (2003 and 2012) and autumn (2014). These seasonal contributions can be explained not by the increasing trend of Asian spring dust, but by seasonal land exposure in coastal regions around southeastern Greenland. Thus, the land exposure in these coastal regions likely increases the supply of local dust to the SE-Dome region and thus increases the nssCa^{2+} flux. In support of this argument, the back trajectory plots show that the southeastern and southern Greenland coastal regions are potential aerosol source regions for the air mass at lower atmosphere (0 and 500 m agl, Figures 2a–2c). Moreover, the Greenland contribution in the 7 and 14 day plots at lower atmosphere (Figure 3) increases after 2000.

3.3. Time Series of Sulfate, Nitrate, and Ammonium Fluxes

The time series of nssSO_4^{2-} , NO_3^- , and NH_4^+ fluxes have generally high contribution during summer (Figure 6), which is a common feature in Greenland ice cores (Fischer et al., 2015; Fuhrer et al., 1996; Geng et al., 2014; Hansson & Holmén, 2001; Silvente & Legrand, 1993). In some periods, such as around 1970 and after 1996, spring and autumn contributions also occur, suggesting an increasing frequency of anthropogenic pollution plumes (Whitlow et al., 1992). As identified in Iizuka et al. (2017), volcanic signals (Figure 1) also appear in spring 1992 (from Pinatubo in the Philippines), in spring 2010 (from Eyjafjallajökull in Iceland), and in autumn–winter 2014 (from Bardarbunga in Iceland).

Overall, the nssSO_4^{2-} flux from 1957 to 2014 (Figure 6a) shows a decreasing trend. But until the mid-1980s, the flux remains within 0.5 to $1.0 \text{ mmol m}^{-2} \text{yr}^{-1}$ with peaks at 1977 ($1.21 \text{ mmol m}^{-2} \text{yr}^{-1}$) and 1984 ($1.18 \text{ mmol m}^{-2} \text{yr}^{-1}$). Then, the flux goes down to about 0.3 to $0.5 \text{ mmol m}^{-2} \text{yr}^{-1}$ except for the volcanic years (1992 and 2014). The peaks at 1977, 1984, 1987, and 1990 arise from spring and/or summer.

The NO_3^- flux from 1957 to 2014 (Figure 6b) is generally constant or

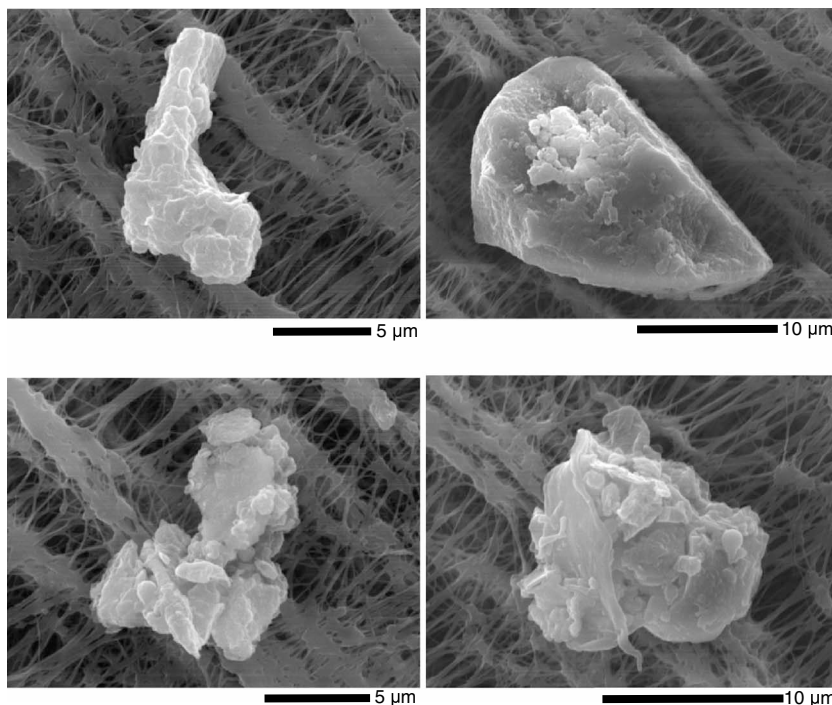


Figure 5. Micrographs of nonvolatile particles on a Teflon filter. The particles were collected from a firn sample in spring 2011, following the sublimation method described in Iizuka et al. (2009, 2012).

3.4. Limited Postdepositional Loss of Nitrate Ions

The postdeposition effect decreases the amount of NO_3^- , particularly at low accumulation rates (Dibb & Jaffrezo, 1997; Geng et al., 2015; Röthlisberger et al., 2002; Wagnon et al., 1999; Zatko et al., 2016). The dependence on accumulation rate (e.g., Röthlisberger et al., 2002; Zatko et al., 2016) occurs because a lower accumulation rate results in a longer exposure time in surface snow, allowing more photolysis and greater evaporation of the snow's impurities (e.g., Wagnon et al., 1999). For NO_3^- , recent studies suggest that photolysis is the main cause of postdepositional loss in Antarctica (Erblund et al., 2013; Frey et al., 2009) and Greenland (Geng et al., 2014). For these reasons, the NO_3^- fluxes in Greenland ice cores depend on the annual accumulation rate (Röthlisberger et al., 2002) (Figure 7a).

At the higher accumulation rates, the NO_3^- flux increases with annual accumulation rate largely because the NO_3^- flux is mainly from wet deposition (Figure 7a). But at low accumulation rates, the postdepositional loss increases the difference between higher and lower accumulation sites. This leads to an expected logarithmic relation between the NO_3^- flux and annual accumulation rate. Indeed, we find that the data well fit such a relation in Figure 7a ($r^2 = 0.93$). In fact, the fits with and without the SE Dome data (not shown) are nearly exactly the same. In the case of Summit, where the accumulation rate is $0.25 \text{ m we yr}^{-1}$ we (Dibb & Fahnestock, 2004), the estimated postdepositional effect ranges from negligible (Fibiger et al., 2013, 2016) to 6% (Geng et al., 2014) and up to 20% (Dibb et al., 2007). The accumulation rate for the SE-Dome ice core is $1.01 \text{ m we yr}^{-1}$, 4 times that at Summit, suggesting that the NO_3^- is preserved without the postdepositional effect. In fact, the NO_3^- flux at SE-Dome's core, $1.13 \text{ mmol m}^{-2} \text{ yr}^{-1}$ (average of 1957–2014), lies on the asymptotic line of the logarithmic curve in Figure 7a.

SE-Dome's high NO_3^- flux is also high for its altitude (Figure 7b) and its latitude (Figure 7c). The NO_3^- flux has no clear relationship with altitude but correlates significantly ($r^2 = 0.54$) with latitude (Figure 7c). The correlation with latitude may suggest that the NO_3^- flux in Greenland is mainly controlled by the location's closeness to the sources in the south and also to North America and Europe, which is consistent with the back trajectory analyses described above (Figure 2). The correlation may also reflect the trend of decreasing accumulation (and hence NO_3^- flux) with latitude in Greenland. The NO_3^- flux at SE-Dome ($1.13 \text{ mmol m}^{-2} \text{ yr}^{-1}$)

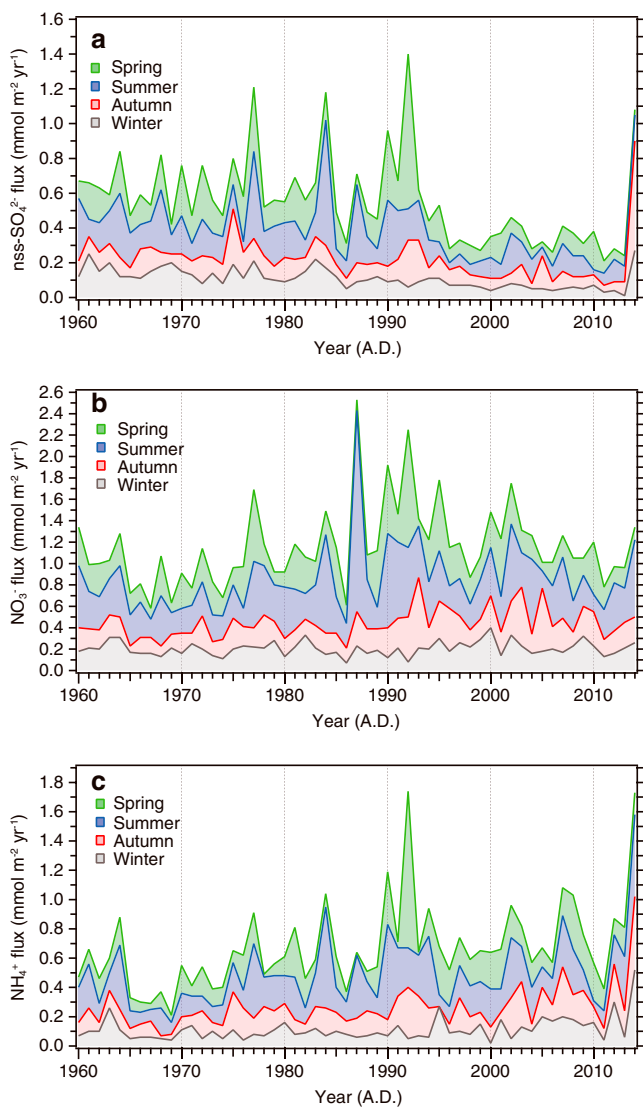


Figure 6. Same as Figure 4, but for (a) nssSO_4^{2-} , (b) NO_3^- , and (c) NH_4^+ .

3.5. Comparison With nssSO_4^{2-} , NO_3^- , and NH_4^+ Fluxes and the EDGAR Emissions

Here we consider how the regional emissions of SO_x , NO_x , and NH_3 , based on the EDGAR 4.3.1 model (Crippa et al., 2016), may have influenced levels at the SE-Dome site. We multiply the regional emissions, shown in Figures 8a–8c, by the regional contributions of air mass in Figure 3, and then consider the relative changes from the 1970–1980 average values.

A 7 day trajectory, as used for Figure 3, is expected to be a median for the aerosol lifetimes of various species. For example, for SO_2 , the lifetime ranges from 13 h (near ground in the U.S.; Lee et al., 2011) to 13 days (Arctic upper troposphere; Höpfner et al., 2015), whereas sulfate is estimated as 8.27 days (Breider et al., 2014), $\text{NH}_3(\text{g})$ as 0.46 days, NH_4^+ as 3.23 days, $\text{HNO}_3(\text{g})$ as 4.76 days, and nitrate as 3.92 days (Xu & Penner, 2012). However, Qi et al. (2017) pointed out that a 7 day trajectory is not sufficient for aerosol transport by an atmospheric model that includes geochemical processes, and they instead considered a 25 day trajectory. To include a range of aerosol behavior, we consider the 7, 14, and 25 day trajectories at the two elevations.

All resulting trajectory cases of 7, 14, and 25 days at the upper and lower elevations show similar trends in Figures 8d–8f. The similarity arises from the similar trends of NO_x and SO_x emissions in North America and

is the highest of all of the cores included in Figure 7. Thus, these data suggest a uniquely high NO_3^- flux regardless of regional differences in depositional settings.

The photolysis of NO_3^- in the snowpack occurs at depths of up to 20 cm (Grannas et al., 2007; Zatko et al., 2013). The snow accumulation at the SE-Dome is 23 cm per month in snow equivalent, as estimated from the surface density of about 360 kg m^{-3} in the ice core (Iizuka et al., 2017). Zatko et al. (2016) showed that the lifetime of photolabile NO_3^- against photolysis is longer than its lifetime in the snow photic zone in southeastern Greenland, which reduces postdepositional photolysis of snow NO_3^- (Figure 10b in Zatko et al., 2016). Such modeling indicates that the photolysis effect around the SE-Dome region is negligible (Figure 10d in Zatko et al., 2016).

In addition, the nitrogen isotopic composition of NO_3^- is consistent with a negligible influence of postdepositional loss of NO_3^- at the SE-Dome region. In a low snow-accumulation site such as East Antarctica ($\sim 10 \text{ cm yr}^{-1}$ snow accumulation), high $\delta^{15}\text{N}$ values of NO_3^- ranging from +50 to +300‰ are observed between the surface and 70 cm depth (Blunier et al., 2005; Frey et al., 2009). The high $\delta^{15}\text{N}$ values result from a combination of a large photolytic loss of NO_3^- and a large isotopic fractionation of NO_3^- photolysis (−40 to −74‰; Frey et al., 2009; Berhanu et al., 2014). In contrast, the $\delta^{15}\text{N}$ value of NO_3^- in surface snow (spring 2015) at the SE-Dome region is only −4.3‰. The $\delta^{15}\text{N}$ (NO_3^-) value of SE-Dome ice equals the lower values measured at Summit, Greenland (−8.7 to 14.3‰, Geng et al., 2014; Fibiger et al., 2016), suggesting no significant influence of postdepositional loss of NO_3^- .

Taken together, the comparison with other ice core data, the modeling, and the low $\delta^{15}\text{N}$ value all show that the SE-Dome region has negligible postdepositional loss of NO_3^- . As the SE-Dome is located in a highland above 3,000 m asl, aerosols are transported from not only local regions around Greenland but also from more distant, remote regions, including nearby continents and oceans. Thus, our results suggest that the SE-Dome region is an excellent region for evaluating and reconstructing nitrate and other volatile material fluxes.

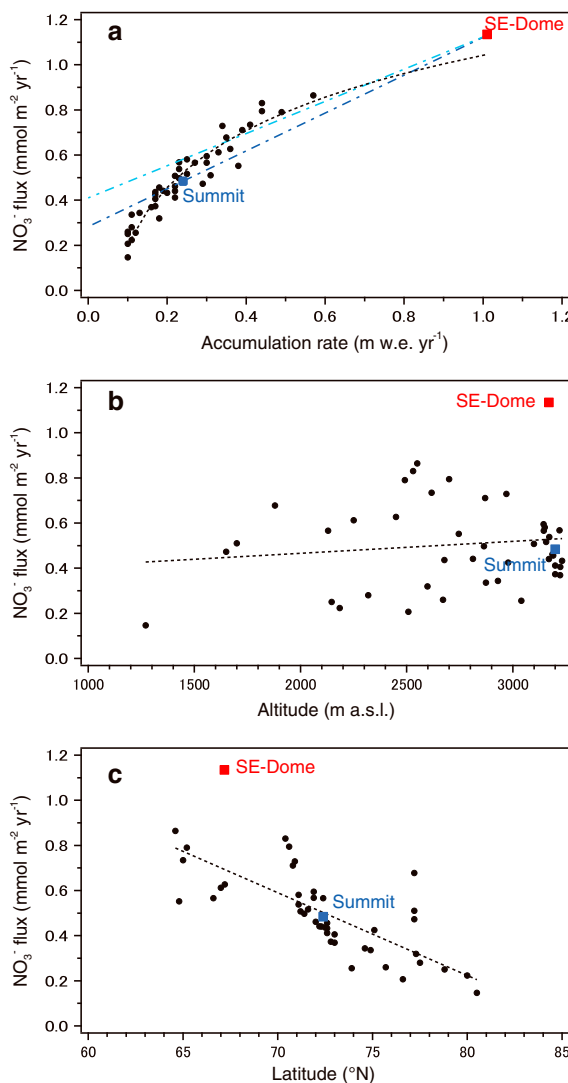


Figure 7. NO₃⁻ flux (m mol m⁻² yr⁻¹) at a range of Greenland sites.
 (a) Dependence on annual accumulation rate (m we yr⁻¹) at the site. The black dashed line shows a regression curve (NO₃⁻ flux = 0.364 × ln (annual accumulation rate) + 1.04), giving a correlation of $r^2 = 0.93$ (P value < 0.01). The dark and light blue lines are lower and upper limit lines for simple accumulation versus NO₃⁻ correlation without postdepositional effect. See text for details.
 (b) Dependence on altitude (m asl) at the site. (c) Dependence on latitude (°N) at the site. The dotted line shows the regression line (NO₃⁻ flux = $-3.67 \cdot 10^{-2} \times (\text{latitude}) + 3.16$), giving a correlation of $r^2 = 0.54$ (P value < 0.01). The black and blue data points are from Röhlisberger et al. (2002).

Europe. The 5 year running averages of nssSO₄²⁻ and NH₄⁺ fluxes in the SE-Dome ice core (black curve) agree well with the regionally weighted SO_x and NH₃ from the EDGAR emissions (red curves). In contrast, the NO₃⁻ flux does not follow the decreasing trend of NO_x emissions very well (Figure 8e). We next consider how two features in the NO₃⁻ flux record (Figure 6b) may explain this discrepancy.

First, note the remarkably high spring and summer contributions to the NO₃⁻ flux peaks from 1985 to 1995 (Figure 6b). During this time, the nssSO₄²⁻, and NH₄⁺ fluxes are also higher than the emission lines (Figure 8). The large NH₄⁺ flux during spring and summer around 1990 (Figure 6c) suggests a forest-fire source because NH₄⁺ spikes in Greenlandic ice cores likely reflect forest fire events in North America (Fischer et al., 2015; Fuhrer et al., 1996; Zennaro et al., 2014). High δ¹⁵N(NO₃⁻) values as well as high concentrations from 1980 to 1990 in Summit ice core also suggested an increase of natural sources like biomass burning (Hastings et al., 2009). Moreover, the forest fire activity increased in the western United States and Canada around 1990 (Fauria & Johnson, 2008; Westerling et al., 2006). Other causes for the NO₃⁻ flux discrepancy include a source region discrepancy between emission and deposition (Lloret & Valiela, 2016) and a change in atmospheric circulation during this period. But forest fires are likely the dominant cause.

Second, despite a clear reduction in NO_x emissions since 1970 in all regions except East Asia, the SE-Dome NO₃⁻ record shows much less decrease after 1996. In fact, the NO₃⁻ flux remains high enough to maintain an average value above the pre-1980 average (Figure 8e). The NO₃⁻ record after 1996 may be explained by a shift in equilibrium driven by a reduction in SO₂ emissions toward more particulate NH₄NO₃ relative to HNO₃. The NH₄NO₃ particles dry deposit only slowly and thus may lead to a longer residence time than nitric acid (Fagerli & Aas, 2008). However, a recent study found a relatively constant summer-particle pH throughout the 15 years of decreasing atmospheric sulfate concentrations, indicating that nitrate is likely to form HNO₃ rather than NH₄NO₃ among the ammonia-sulfate-nitrate system (Weber et al., 2016). The gaseous HNO₃ also reacts with sea salt (Na⁺) and dust (nssCa²⁺). In fact, Na⁺ and nssCa²⁺ fluxes increased after 2000, whereas the nssSO₄²⁻ flux decreased after the mid-1990s (section 3.3). In such an ion balance, the formation of NaNO₃ and Ca(NO₃)₂ may accelerate and may lead to a longer residence time. Thus, several chemical processes during transport may be involved. Clearly, a comprehensive understanding of the NO₃⁻ record in the SE-Dome ice core requires a more complete atmospheric model that includes detailed atmospheric chemical processes (section 3.6).

Finally, variations in regional deposition may be important. For example, nitrate in precipitation in Europe decreased by 25% overall since 1990, but the variation from country to country is large (Tørseth et al., 2012). In North America, a recent compilation of nitrogen oxide deposition revealed that the regional-scale variations are highly affected by emission from, and transport through, neighboring source areas (Lloret & Valiela, 2016). Concerning historical changes, in Europe, despite a 31% reduction of NO_x emission from 1990 to 2009, the concentrations of total airborne nitrate decreased only 8% (Tørseth et al., 2012). In North America, during 1980–2000, only minor changes and even increases were observed at some sites, then, after 2000, most sites showed significant decreasing trends (Lloret & Valiela, 2016).

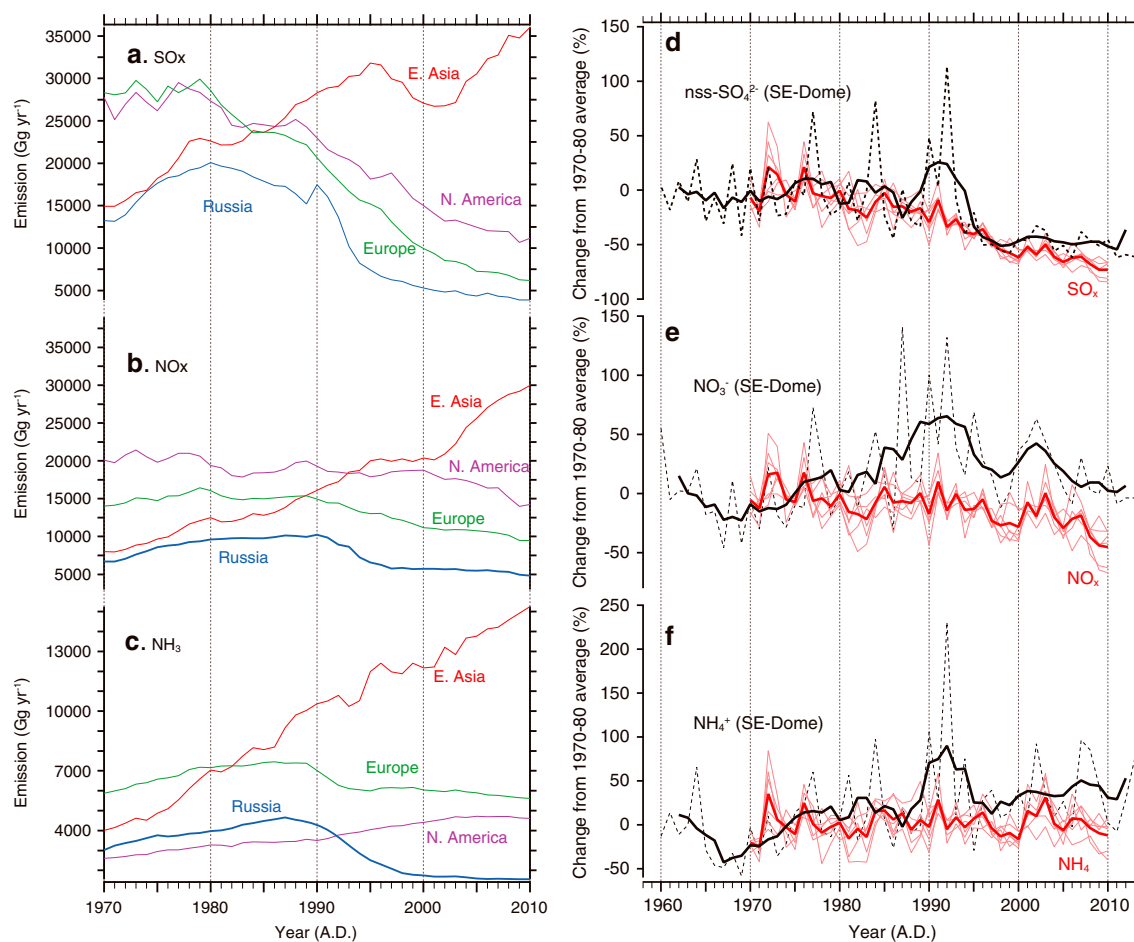


Figure 8. Emission and back trajectory trends. (a–c) Emission-source trends (Gg yr^{-1}) from four land regions. North America (purple) is Canada and the U.S., Europe (green) includes all of Europe, Russia (blue) is Russia and the Ukraine, and East Asia (red) is China and Japan. (a) SO_x emissions. (b) NO_x emissions. (c) NH_3 emissions. (Values from Greenland are negligible on this scale.) The SO_x , NO_x , and NH_3 emission data are from the Emission Database for Global Atmospheric Research (EDGAR, release version 4.3.1.) from the European Commission, Joint Research Centre (JRC)/Netherlands Environmental Assessment Agency (PBL). Ion-flux trends and various emission-source trends normalized to the 1970–1980 averages. The annual ion fluxes are based on the annual accumulation rate and here have the boundary of 1 January. (d) Normalized nssSO_4^{2-} fluxes at the SE-Dome ice core (black dashed line) and regional contributions of EDGAR SO_x emissions (each of the six thin red lines is from a case in Figures 2a–2f) transported to the SE-Dome region site. The red thick line is the average trend of the six thin lines. The black solid line is the 5 year running mean of the fluxes. (e) NO_3^- flux and NO_x emissions; (f) NH_4^+ flux and NH_3 emissions.

Overall, the inconsistency between SE-Dome NO_3^- flux and the NO_x emission record suggests that the NO_3^- flux record reflects the combined effect of changes in NO_x emissions in source areas, transport of air masses from source areas, and atmospheric chemical processes during transport. In contrast, the SO_x and NH_3 records based on emissions and air mass contributions (Figure 8) agree well with the nssSO_4^{2-} and NH_4^+ fluxes. This result suggests that unique and complex atmospheric chemical processes (i.e., preferential scavenging and/or sustaining) may have a larger influence on NO_3^- than for nssSO_4^{2-} and NH_4^+ .

3.6. Limitations of the Emission and Trajectory Analyses

A limitation of these arguments (section 3.5) is that the back trajectory analysis estimates the transport of the air parcel, not the aerosol itself. For example, the 25 day trajectory plot in Figure 2f suggests a contribution from Alaska. Such a contribution of nitrate may have come from Asian nitrate that transports to the North Pacific Ocean via peroxyacetyl nitrate formation (e.g., Brock et al., 2004; Dunlea et al., 2009). In this case, we should account for NO_x being a short-lived radical that influences the oxidizing capacity of the atmosphere via interactions with ozone (O_3) and hydroxyl radical (OH). But we do not consider these reactions in detail here.

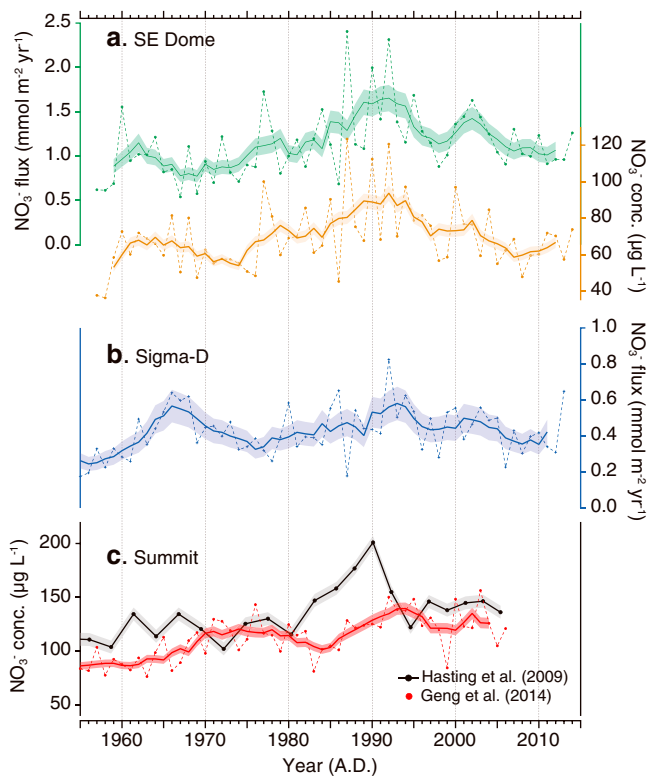


Figure 9. Time series of NO_3^- fluxes or concentrations at three core sites in Greenland. (a) Flux and concentration at SE-Dome, both of which here have the boundary of 1 January (southeast Greenland). (b) Flux at SIGMA-D (northwest Greenland). The dashed lines are raw flux/concentration data, and the solid lines are the 5 year running means with error range of about 16 and 9% for flux and concentration, respectively. (c) NO_3^- concentrations ($\mu\text{g kg}^{-1}$) of two Summit (central Greenland) ice cores. The black line is from Hastings et al. (2009) with error range of 6 ppb. The dotted red line is from Geng et al. (2014). The solid red line is the 5 year running mean with an error range of about 4% based on a 10% uncertainty in NO_3^- concentration.

in 1985–1995 and (2) levels in 1996 to 2014 at or above those during 1960–1980. We assume that years with a lower annual accumulation would have had a greater postdepositional effect. In such years, the NO_3^- may not be a good proxy of dry/wet deposition. Thus, for the summit data in Figure 9, the NO_3^- concentration trend may differ between them and from the flux trend. However, the similar features among the three data sets indicate that these cores well preserve past NO_3^- fluctuations over more than a decade. About $0.25 \text{ m we yr}^{-1}$ of annual accumulation is typical over Greenland (Figure 7a), and the regions of some deep ice cores (e.g., GRIP, NGRIP, GISP2, and NEEM) so far obtained have about the same accumulation rate during the Holocene. However, the Dye 3 deep ice core has $0.49 \text{ m we yr}^{-1}$ of annual accumulation and may have an advantage for discussing nitrate fluctuation from the last glacial period to the Holocene. Our results for the SE-Dome ice core, an excellent location for evaluating and reconstructing nitrate fluxes, guarantee the reliability of NO_3^- concentrations as the proxy of dry/wet deposition of general ice cores in Greenland over decadal or longer time scales.

4. Summary

We have shown that the high-accumulation rate of the SE-Dome region ($1.01 \text{ m we yr}^{-1}$) makes it an excellent location for evaluating and reconstructing ion fluxes, especially nitrate. The Cl^- , Na^+ , and Mg^{2+} ions were mainly from sea salt, all having winter maxima. For nssCa^{2+} , an increasing trend after 2000 could be explained as coming from the local dust around southeastern Greenland. The nssSO_4^{2-} flux had a maximum during the 1960s–1970s but decreased after 1970–1980, indicating a proxy of anthropogenic SO_x . In contrast, the NH_4^+

Also, one should consider the possibility of wet deposition prior to air mass arrival at the site. For example, compound removal via precipitation scavenging during transport can occur but is not included in the trajectory modeling. In future studies, our NO_3^- , nssSO_4^{2-} , and NH_4^+ data set may be useful for testing the more detailed chemical transportation models, such as GEOS-Chem (<http://acmg.seas.harvard.edu/geos/index.html>). However, current chemical transport models in the Arctic are not yet well-designed for reactive gases (e.g., Emmons et al., 2015) and aerosols (e.g., Eckhardt et al., 2015).

3.7. Comparison With Ice Cores From Low-Accumulation Regions

The NO_3^- flux linearly correlates with the annual accumulation rate because the NO_3^- falls mainly through wet deposition. The dark-blue line in Figure 7a connects the SE-Dome ice core and the summit core values. If the NO_3^- flux in the summit core is unaffected by postdepositional loss (Fibiger et al., 2013, 2016), then the resulting line would represent a lower-limit line for simple accumulation versus NO_3^- correlation without postdepositional effect. But if, as suggested by Dibb et al. (2007), a 20% loss in NO_3^- occurs at summit via postdepositional processes, then the line connecting SE-Dome data and the point 1.2 times the NO_3^- flux at summit would represent an upper limit of the postdepositional effect (the light blue line in Figure 7a). The intersection of these two lines with the data-fit curve (dashed black) suggests that the postdepositional effect on NO_3^- would be negligible in an ice core drilling site with accumulation rate exceeding $0.19\text{--}0.36 \text{ m we yr}^{-1}$.

Finally, we compare the SE Dome's NO_3^- concentration/flux after 1950 to those of two other Greenland sites. Both the NO_3^- concentration and flux trends are quite similar. The profiles in Figure 9 show that the peak levels and annual variations differ among the three sites, yet their 5 year running means show a similar trend despite the low annual accumulation in the Summit (central Greenland) and SIGMA-D (northwest Greenland) ice cores (both about $0.25 \text{ m we yr}^{-1}$). These NO_3^- concentration/flux records have two common features: (1) large peaks

flux increased during 1957–2014, indicating a proxy of NH_3 emissions. The NO_3^- flux was about $1.13 \text{ mmol m}^{-2} \text{ yr}^{-1}$ ($68.9 \mu\text{g L}^{-1}$ concentration) with negligible postdepositional influences. This flux did not follow the decreasing trend of NO_x emissions, differing in two ways. First, large spikes in the flux were detected from 1985 to 1995. Second, the NO_3^- flux from 1996 to 2014 was roughly constant and slightly higher compared with that from the 1960s to the 1980s, a time period when the anthropogenic NO_x emission was higher. The NO_3^- fluxes/concentrations in some Greenland ice cores have a low accumulation rate ($\sim 0.25 \text{ m we yr}^{-1}$) yet show similar features as those at the SE-Dome ice core, suggesting that NO_3^- concentrations may be a reliable proxy of wet deposition of ice cores in Greenland over decadal time scales. In the near future, the relationships between NO_x , NH_3 , and SO_x emissions and the NO_3^- , NH_4^+ , and nssSO_4^{2-} fluxes should be quantified using atmospheric aerosol models. The data provided here may help in such efforts.

Acknowledgments

The authors gratefully acknowledge the Air Resources Laboratory (ARL) for the provision of the HYSPLIT transport and dispersion model on the READY Web site (<http://www.arl.noaa.gov/ready.html>) and the Joint Research Centre (JRC; <http://edgar.jrc.ec.europa.eu/>) for provision of EDGARv4.3.1 emission data used in this publication. We are grateful to the drilling and initial analysis teams of SE-Dome ice. The paper was significantly improved as a result of comments, especially on aerosol pH and source interpretation by Weber et al. (2016) and three anonymous referees and the handling by Scientific Editor L. Russell, to whom we are greatly indebted. This study was supported by MEXT/JSPS KAKENHI grants 26257201, 16 K12573, 17H06105, and 16H05884; the Joint Research Program of the Institute of Low Temperature Science, Hokkaido University; and the Readership Program of the Institute of Low Temperature Science, Hokkaido University. This study is partly responsible for ArCS (Arctic Challenge for Sustainability Project). The data used in this study will be available in the Hokkaido University Collection of Scholarly and Academic papers (<http://hdl.handle.net/2115/67885>).

References

- Andreae, M. O., & Rosenfeld, D. (2008). Aerosol-cloud-precipitation interactions. Part 1. The nature and sources of cloud-active aerosols. *Earth-Science Reviews*, 89, 13–41.
- Berhanu, T. A., Meusinger, C., Erbland, J., Jost, R., Bhattacharya, S. K., Johnson, M. S., & Savarino, J. (2014). Laboratory study of nitrate photolysis in Antarctic snow. II. Isotopic effects and wavelength dependence. *The Journal of Chemical Physics*, 140, 244306. <https://doi.org/10.1063/1.4882899>
- Bjørk, A. A., Kjær, K. H., Korsgaard, N. J., Khan, S. A., Kjeldsen, K. K., Andresen, C. S., ... Funder, S. (2012). An aerial view of 80 years of climate-related glacier fluctuations in southeast Greenland. *Nature Geoscience*, 5, 427–432. <https://doi.org/10.1038/NGE01481>
- Blunier, T., Floch, G. L., Jacobi, H.-W., & Quansah, E. (2005). Isotopic view on nitrate loss in Antarctic surface snow. *Geophysical Research Letters*, 32, L13501. <https://doi.org/10.1029/2005GL023011>
- Bory, A. J.-M., Biscaye, P. E., Piotrowski, A. M., & Steffensen, J. P. (2003). Regional variability of ice core dust composition and provenance in Greenland. *Geochemistry, Geophysics, Geosystems*, 4(12), 1107. <https://doi.org/10.1029/2003GC000627>
- Breider, T. J., Mickley, L. J., Jacob, D. J., Wang, Q., Fisher, J. A., Chang, R. Y.-W., & Alexander, B. (2014). Annual distributions and sources of Arctic aerosol components, aerosol optical depth, and aerosol absorption. *Journal of Geophysical Research: Atmospheres*, 119, 4107–4124. <https://doi.org/10.1002/2013JD020996>
- Brock, C. A., Hudson, P. K., Lovejoy, E. R., Sullivan, A., Nowak, J. B., Huey, L. G., ... Wilson, J. C. (2004). Particle characteristics following cloud-modified transport from Asia to North America. *Journal of Geophysical Research*, 109, D23S26. <https://doi.org/10.1029/2003JD004198>
- Crippa, M., Janssens-Maenhout, G., Dentener, F., Guizzardi, D., Sindelarova, K., Muntean, M., ... Granier, C. (2016). Forty years of improvements in European air quality: Regional policy-industry interactions with global impacts. *Atmospheric Chemistry and Physics*, 16, 3825–3841. <https://doi.org/10.5194/acp-16-3825-2016>
- Dee, D. P., Uppala, S. M., Simmons, A. J., Berrisford, P., Poli, P., Kobayashi, S., ... Vitart, F. (2011). The ERA-Interim reanalysis: Configuration and performance of the data assimilation system. *Quarterly Journal of the Royal Meteorological Society*, 137, 553–597. <https://doi.org/10.1002/qj.828>
- Dibb, J. E., & Fahnestock, M. (2004). Snow accumulation, surface height change, and firn densification at Summit, Greenland: Insights from 2 years of in situ observation. *Journal of Geophysical Research*, 109, D24113. <https://doi.org/10.1029/2003JD004300>
- Dibb, J. E., & Jaffrezo, J. L. (1997). Air-snow exchange investigations at Summit, Greenland: An overview. *Journal of Geophysical Research*, 102(C12), 26,795–26,807. <https://doi.org/10.1029/96JC02303>
- Dibb, J. E., Whitlow, S. I., & Arsenault, M. (2007). Seasonal variations in the soluble ion content of snow at Summit, Greenland: Constraints from three years of daily surface snow samples. *Atmospheric Environment*, 41(24), 5007–5019.
- Dunlea, E. J., DeCarlo, P. F., Aiken, A. C., Kimmel, J. R., Peltier, R. E., Weber, R. J., ... Jimenez, J. L. (2009). Evolution of Asian aerosols during transpacific transport in INTEX-B. *Atmospheric Chemistry and Physics*, 9(19), 7257–7287. <https://doi.org/10.5194/acp-9-7257-2009>
- Eckhardt, S., Quennhenen, B., Olivié, D. J. L., Berntsen, T. K., Cherian, R., Christensen, J. H., ... Stohl, A. (2015). Current model capabilities for simulating black carbon and sulfate concentrations in the Arctic atmosphere: A multi-model evaluation using a comprehensive measurement data set. *Atmospheric Chemistry and Physics*, 15, 9413–9433. Retrieved from www.atmos-chem-phys.net/15/9413/2015/ doi:10.5194/acp-15-9413-2015
- Emmons, L. K., Arnold, S. R., Monks, S. A., Huijnen, V., Tilmes, S., Law, K. S., ... Helmig, D. (2015). The POLARCAT Model Intercomparison Project (POLMIP): Overview and evaluation with observations. *Atmospheric Chemistry and Physics*, 15, 6721–6744. <https://doi.org/10.5194/acp-15-6721-2015>
- EPICA community members (2004). Eight glacial cycles from an Antarctic ice core. *Nature*, 429, 623–628. <https://doi.org/10.1038/nature02599>
- EPICA community members (2006). One-to-one coupling of glacial climate variability in Greenland and Antarctica. *Nature*, 444, 195–198. <https://doi.org/10.1038/nature05301>
- Erbland, J., Vicars, W. C., Savarino, J., Morin, S., Frey, M. M., Frosini, D., ... Martins, J. M. F. (2013). Air-snow transfer of nitrate on the East Antarctic Plateau—Part 1: Isotopic evidence for a photolytically driven dynamic equilibrium in summer. *Atmospheric Chemistry and Physics*, 13, 6403–6419. <https://doi.org/10.5194/acp-13-6403-2013>
- Fagerli, H., & Aas, W. (2008). Trends of nitrogen in air and precipitation: Model results and observations at EMEP sites in Europe, 1980–2003. *Environmental Pollution*, 154(2008), 448–461.
- Fauria, M. M., & Johnson, E. A. (2008). Climate and wildfire in the North American boreal forest. *Philosophical Transactions of the Royal Society B*, 363, 2317–2329.
- Fibiger, D. L., Hastings, M. G., Dibb, J. E., & Huey, L. G. (2013). The preservation of atmospheric nitrate in snow at Summit, Greenland. *Geophysical Research Letters*, 40, 3484–3489.
- Fibiger, D. L., Dibb, J. E., Chen, D., Thomas, J. L., Burkhardt, J. F., Huey, L. G., & Hastings, M. G. (2016). Analysis of nitrate in the snow and atmosphere at Summit, Greenland: Chemistry and transport. *Journal of Geophysical Research: Atmospheres*, 121, 5010–5030. <https://doi.org/10.1002/2015JD024187>
- Fischer, H., Wagenbach, D., & Kipfstuhl, J. (1998). Sulfate and nitrate firn concentrations on the Greenland ice sheet: 2. Temporal anthropogenic deposition changes. *Journal of Geophysical Research*, 103(D17), 21,935–21,942. <https://doi.org/10.1029/98JD01886>

- Fischer, H., Siggaard-Andersen, M.-L., Ruth, U., Röhlisberger, R., & Wolff, E. (2007). Glacial/interglacial changes in mineral dust and sea-salt records in polar ice cores: Sources, transport and deposition. *Reviews of Geophysics*, 45, RG1002. <https://doi.org/10.1029/2005RG000192>
- Fischer, H., Schüpbach, S., Gfeller, G., Bigler, M., Röhlisberger, R., Erhardt, T., ... Wolff, E. (2015). Millennial changes in North American wildfire and soil activity over the last glacial cycle. *Nature Geoscience*, 8, 723–727. <https://doi.org/10.1038/ngeo2495>
- Frey, M. M., Savarino, J., Morin, S., Erbland, J., & Martins, J. M. F. (2009). Photolysis imprint in the nitrate stable isotope signal in snow and atmosphere of East Antarctica and implications for reactive nitrogen cycling. *Atmospheric Chemistry and Physics*, 9, 8681–8696.
- Fuhrer, K., Neftel, A., Anklan, M., Staffelbach, T., & Legrand, M. (1996). High-resolution ammonium ice core record covering a complete glacial-interglacial cycle. *Journal of Geophysical Research*, 101(D12), 4147–4164. <https://doi.org/10.1029/95JD02903>
- Furukawa, R., Uemura, R., Fujita, K., Sjolte, J., Yoshimura, K., Matoba, S., & Iizuka, Y. (2017). Seasonal scale dating of shallow ice core from Greenland using oxygen isotope matching between data and simulation. *Journal of Geophysical Research: Atmospheres*, 122, 10,873–10,887. <https://doi.org/10.1002/2017JD026716>
- Geng, L., Cole-Dai, J., Alexander, B., Erbland, J., Savarino, J., Schauer, A. J., ... Zatko, M. C. (2014). On the origin of the occasional spring nitrate peak in Greenland snow. *Atmospheric Chemistry and Physics*, 14, 13,361–13,376. <https://doi.org/10.5194/acp-14-13361-2014>
- Geng, L., Zatko, M. C., Alexander, B., Fudge, T. J., Schauer, A. J., Murray, L. T., & Mickley, L. J. (2015). Effects of post depositional processing on nitrogen isotopes of nitrate in the Greenland Ice Sheet Project 2 ice core. *Geophysical Research Letters*, 42, 5346–5354. <https://doi.org/10.1002/2015GL064218>
- Grannas, A. M., Jones, A. E., Dibb, J., Ammann, M., Anastasio, C., Beine, H. J., ... Zhu, T. (2007). An overview of snow photochemistry: Evidence, mechanisms and impacts. *Atmospheric Chemistry and Physics*, 7, 4329–4373. <https://doi.org/10.5194/acp-7-4329-2007>
- Greenland Ice-core Project Members (1993). Climate instability during the last interglacial period recorded in the GRIP ice core. *Nature*, 364, 203–207.
- Grootes, P. M., Stuiver, M., White, J. W. C., Johnsen, S., & Jouzel, J. (1993). Comparison of oxygen isotope records from the GISP2 and GRIP Greenland ice cores. *Nature*, 366, 552–554. <https://doi.org/10.1038/366552a0>
- Hanna, E., McConnell, J., Das, S., Cappelen, J., & Stephens, A. (2006). Observed and modeled Greenland ice sheet snow accumulation, 1958–2003, and links with regional climate forcing. *Journal of Climate*, 19, 344–358.
- Hansson, M., & Holmén, K. (2001). High latitude biospheric activity during the last glacial cycle revealed by ammonium variations in Greenland ice cores. *Geophysical Research Letters*, 28(22), 4239–4242. <https://doi.org/10.1029/2000GL01231>
- Hastings, M. G., Jarvis, J. C., & Steig, E. J. (2009). Anthropogenic impacts on nitrogen isotopes of ice-core nitrate. *Science*, 324(5932), 1288.
- Hattori, S., Savarino, J., Kamezaki, K., Ishino, S., Dyckmans, J., Fujinawa, T., ... Yoshida, N. (2016). Automated system measuring triple oxygen and nitrogen isotope ratios in nitrate using the bacterial method and N_2O decomposition by microwave discharge. *Rapid Communications in Mass Spectrometry*, 30, 2635–2644. <https://doi.org/10.1002/rcl.7747>
- Höpfner, M., Boone, C. D., Funke, B., Glatthor, N., Grabowski, U., Günther, A., ... Wissmüller, K. (2015). Sulfur dioxide (SO_2) from MIPAS in the upper troposphere and lower stratosphere 2002–2012. *Atmospheric Chemistry and Physics*, 15, 7017–7037.
- Iizuka, Y., Fujii, Y., Hirasawa, N., Suzuki, T., Motoyama, H., Furukawa, T., & Hondoh, T. (2004). SO_4^{2-} minimum in summer snow layer at Dome Fuji, Antarctica and the probable mechanism. *Journal of Geophysical Research*, 109, D04307. <https://doi.org/10.1029/2003JD004138>
- Iizuka, Y., Miyake, T., Hirabayashi, M., Suzuki, T., Matoba, S., Motoyama, H., ... Hondoh, T. (2009). Constituent elements of insoluble and nonvolatile particles during the Last Glacial Maximum of the Dome Fuji ice core. *Journal of Glaciology*, 55(191), 552–562.
- Iizuka, Y., Uemura, R., Motoyama, H., Suzuki, T., Miyake, T., Hirabayashi, M., & Hondoh, T. (2012). Sulfate-climate coupling over the past 300,000 years in inland Antarctica. *Nature*, 490, 81–84. <https://doi.org/10.1038/nature11359>
- Iizuka, Y., Matoba, S., Yamasaki, T., Oyabu, I., Kadota, M., & Aoki, T. (2016). Glaciological and meteorological observations at the SE-Dome site, southeastern Greenland Ice Sheet. *Bulletin of Glaciological Research*, 34, 1–10. <https://doi.org/10.5331/bgr.15R03>
- Iizuka, Y., Miyamoto, A., Hori, A., Matoba, S., Furukawa, R., Saito, T., ... Takeuchi, N. (2017). A firn densification process in the high accumulation dome of southeastern Greenland. *Arctic, Antarctic, and Alpine Research*, 49, 13–27. <https://doi.org/10.1657/AAAR0016-034>
- IPCC (2013). Climate change 2013: The physical science basis. In T. F. Stocker, et al. (Eds.), *Contribution of working group I to the fifth assessment report of the Intergovernmental Panel on Climate Change* (Chap. 8, p. 1535). Cambridge, United Kingdom and New York: Cambridge University Press. <https://doi.org/10.1017/CBO978107415324>
- Ishino, S., Hattori, S., Savarino, J., Jourdain, B., Preunkert, S., Legrand, M., ... Yoshida, N. (2017). Seasonal variations of triple oxygen isotopic compositions of atmospheric sulfate, nitrate and ozone at Dumont d'Urville, coastal Antarctica. *Atmospheric Chemistry and Physics*, 17, 3713–3727. <https://doi.org/10.5194/acp-17-3713-2017>
- Lee, C., Martin, R. V., van Donkelaar, A., Lee, H., Dickerson, R. R., Hains, J. C., ... Schwab, J. L. (2011). SO_2 emissions and lifetimes: Estimates from inverse modeling using in situ and global, space-based (SCIAMACHY and OMI) observations. *Journal of Geophysical Research*, 116, D06304. <https://doi.org/10.1029/2010JD014758>
- Legrand, M. R., & Mayewski, P. (1997). Glaciochemistry of polar ice cores: A review. *Reviews of Geophysics*, 35(3), 219–244.
- Legrand, M. R., Loria, C., Barkov, N. I., & Petrov, V. N. (1988). Vostok (Antarctica) ice core: Atmospheric chemistry changes over the last climatic cycle (160,000 years). *Atmospheric Environment*, 22(2), 317–331.
- Likens, G. E., Driscoll, C. T., & Buso, D. C. (1996). Long-term effects of acid rain: Response and recovery of a forest ecosystem. *Science*, 272(5259), 244–246. <https://doi.org/10.1126/science.272.5259.244>
- Lloret, J., & Valiela, I. (2016). Unprecedented decrease in deposition of nitrogen oxides over North America: The relative effects of emission controls and prevailing air-mass trajectories. *Biogeochemistry*, 129, 165–180. <https://doi.org/10.1007/s10533-016-0225-5>
- Maselli, O. J., Chellman, N. J., Grieman, M., Layman, L., McConnell, J. R., Pasteris, D., ... Sigl, M. (2017). Sea ice and pollution-modulated changes in Greenland ice core methane sulfonate and bromine. *Climate of the Past*, 13, 39–59. <https://doi.org/10.5194/cp-13-39-2017>
- Matoba, T., Motoyama, H., Fujita, K., Yamasaki, T., Minowa, M., Onuma, Y., ... Enomoto, H. (2015). Glaciological and meteorological observations at the SIGMA-D site, northwestern Greenland Ice Sheet. *Bulletin of Glaciological Research*, 33, 7–14. <https://doi.org/10.5331/bgr.33.7>
- Moore, G. W. K., Renfrew, I. A., Harden, B. E., & Mernild, S. H. (2015). The impact of resolution on the representation of southeast Greenland barrier winds and katabatic flows. *Geophysical Research Letters*, 42, 3011–3018. <https://doi.org/10.1002/2015GL063550>
- Nagashima, K., Suzuki, Y., Irino, T., Nakagawa, T., Tada, R., Hara, Y., ... Kurosaki, Y. (2016). Asian dust transport during the last century recorded in Lake Suigetsu sediments. *Geophysical Research Letters*, 43, 2835–2842.
- North Greenland Ice Core Project Members (2004). High-resolution record of Northern Hemisphere climate extending into the last interglacial period. *Nature*, 431, 147–151. <https://doi.org/10.1038/nature02805>
- Patrissi, N., Delmas, R. J., Legrand, M., De Angelis, M., Ferron, F. A., Stiévenard, M., & Jouzel, J. (2002). First sulfur isotope measurements in central Greenland ice cores along the preindustrial and industrial periods. *Journal of Geophysical Research*, 107(D11). <https://doi.org/10.1029/2001JD000672>

- Petit, J. R., Jouzel, J., Raynaud, D., Barkov, N. I., Barnola, J. M., Basile, I., ... Stievenard, M. (1999). Climate and atmospheric history of the past 420,000 years from the Vostok ice core, Antarctica. *Nature*, 399, 429–436.
- Plummer, C. T., Curran, M. A. J., van Ommen, T. D., Rasmussen, S. O., Moy, A. D., Vance, T. R., ... Mayewski, P. A. (2012). An independently dated 2000-yr volcanic record from Law Dome, East Antarctica, including a new perspective on the dating of the 1450s CE eruption of Kuwae, Vanuatu. *Climate of the Past*, 8, 1929–1940. <https://doi.org/10.5194/cp-8-1929-2012>
- Pöschl, U. (2005). Atmospheric aerosols: Composition, transformation (2005), climate and health effects. *Angewandte Chemie, International Edition*, 44, 7520–7540. <https://doi.org/10.1002/anie.200501122>
- Prospero, J. M., Ginoux, P., Torres, O., Nicholson, S. E., & Gill, T. E. (2002). Environmental characterization of global sources of atmospheric soil dust identified with the Nimbus 7 total ozone mapping spectrometer (TOMS) absorbing aerosol product. *Reviews of Geophysics*, 40(1), 1002. <https://doi.org/10.1029/2000RG000095>
- Qi, L., Li, Q., Henze, D. K., Tseng, H.-L., & He, C. (2017). Sources of springtime surface black carbon in the Arctic: An adjoint analysis for April 2008. *Atmospheric Chemistry and Physics*, 17, 9697–9716. <https://doi.org/10.5194/acp-17-9697-2017>
- Röhlisberger, R., Hutterli, M. A., Wolff, E. W., Mulvaney, R., Fischer, H., Bigler, M., ... Steffensen, J. P. (2002). Nitrate in Greenland and Antarctic ice cores: A detailed description of post-depositional processes. *Annals of Glaciology*, 35, 209–216.
- Silvente, E., & Legrand, M. (1993). Ammonium to sulfate ratio in aerosol and snow of Greenland and Antarctic regions. *Geophysical Research Letters*, 20(8), 687–690. <https://doi.org/10.1029/93GL00982>
- Stein, A. F., Draxler, R. R., Rolph, G. D., Stunder, B. J. B., Cohen, M. D., & Ngan, F. (2015). NOAA's HYSPLIT Atmospheric Transport and Dispersion Modeling System. *Bulletin of the American Meteorological Society*, 96(12), 2059–2077. <https://doi.org/10.1175/BAMS-D-14-00110.1>
- Stoddard, J. L., Jeffries, D. S., Lükewille, A., Clair, T. A., Dillon, P. J., Driscoll, C. T., ... Wilander, A. (1999). Regional trends in aquatic recovery from acidification in North America and Europe. *Nature*, 401, 575–578. <https://doi.org/10.1038/44114>
- Tørseth, K., Aas, W., Breivik, K., Fjæraa, A. M., Fiebig, M., Hjellbrekke, A. G., ... Yttri, K. E. (2012). Introduction to the European Monitoring and Evaluation Programme (EMEP) and observed atmospheric composition change during 1972–2009. *Atmospheric Chemistry and Physics*, 12, 5447–5481. <https://doi.org/10.5194/acp-12-5447-2012>
- Uppala, S. M., Källberg, P. W., Simmons, A. J., Andrae, U., Da Costa Bechtold, V., Fiorino, M., ... Woollen, J. (2005). The ERA-40 re-analysis. *Quarterly Journal of the Royal Meteorological Society*, 131, 2961–3012.
- van den Broeke, M., Bamber, M. J., Ettema, J., Rignot, E., Schrama, E., van de Berg, W. J., ... Wouters, B. (2009). Partitioning recent Greenland mass loss. *Science*, 326, 984–986.
- Wagnon, P., Delmas, R. J., & Legrand, M. (1999). Loss of volatile acid species from upper firn layers at Vostok, Antarctica. *Journal of Geophysical Research*, 104(D3), 3423–3431.
- Watanabe, O., Jouzel, J., Johnsen, S., Parrenin, F., Shoji, H., & Yoshida, N. (2003). Homogeneous climate variability across East Antarctica over the past three glacial cycles. *Nature*, 422(6931), 509–512. <https://doi.org/10.1038/nature01525>
- Weber, R. J., Guo, H., Russell, A. G., & Nenes, A. (2016). High aerosol acidity despite declining atmospheric sulfate concentrations over the past 15 years. *Nature Geoscience*, 9, 282–285. <https://doi.org/10.1038/NGEO2665>
- Westerling, A. L., Hidalgo, H. G., Cayan, D. R., & Swetnam, T. W. (2006). Warming and earlier spring increase western U.S. forest wildfire activity. *Science*, 313(5789), 940–943. <https://doi.org/10.1126/science.1128834>
- Whitlow, S., Mayewski, P. A., & Dibb, J. E. (1992). A comparison of major chemical species seasonal concentration and accumulation at the South Pole and Summit, Greenland. *Atmospheric Environment*, 26A(11), 2045–2054.
- Wolff, E. W., Fischer, H., Fundel, F., Ruth, U., Twarloh, B., Littot, G. C., ... Gaspari, V. (2006). Southern Ocean sea-ice extent, productivity and iron flux over the past eight glacial cycles. *Nature*, 440, 491–496.
- Xu, L., & Penner, J. E. (2012). Global simulations of nitrate and ammonium aerosols and their radiative effects. *Atmospheric Chemistry and Physics*, 12, 9479–9504. <https://doi.org/10.5194/acp-12-9479-2012>
- Zatko, M. C., Grenfell, T. C., Alexander, B., Doherty, S. J., Thomas, J. L., & Yang, X. (2013). The influence of snow grain size and impurities on the vertical profiles of actinic flux and associated NOx emissions on the Antarctic and Greenland ice sheets. *Atmospheric Chemistry and Physics*, 13, 3547–3567. <https://doi.org/10.5194/acp-13-3547-2013>
- Zatko, M., Geng, L., Alexander, B., Sofen, E., & Klein, K. (2016). The impact of snow nitrate photolysis on boundary layer chemistry and the recycling and redistribution of reactive nitrogen across Antarctica and Greenland in a global chemical transport model. *Atmospheric Chemistry and Physics*, 16, 2819–2842. <https://doi.org/10.5194/acp-16-2819-2016>
- Zennaro, P., Kehrwald, N., McConnell, J. R., Schuepbach, S., Maselli, O. J., Marlon, J., ... Barbante, C. (2014). Fire in ice: Two millennia of boreal forest fire history from the Greenland NEEM ice core. *Climate of the Past*, 10, 1905–1924.
- Zhu, C., Wang, B., & Qian, W. (2008). Why do dust storms decrease in northern China concurrently with the recent global warming? *Geophysical Research Letters*, 35, L18702. <https://doi.org/10.1029/2008GL034886>